Original Article

Applying XFEM Analysis and Stochastic Approaches to Interfacial Crack Modeling in Bimaterial Systems with **Void Inclusions**

M B Vaghela¹, Markad Kanif², Jay M. Pujara³, C A Maradiya⁴, J H Solanki⁵, D B Patel⁶

1,3,4,5,6 Mechanical Engineering Department, Lukhdhirji Engineering College, Morbi, Gujarat, India. ²Department of Mechanical Engineering, DVVP College of Engineering, Ahmednagar, Maharashtra, India.

¹Corresponding Author: manoj0085@gmail.com

Received: 06 August 2025 Revised: 07 September 2025 Accepted: 08 October 2025 Published: 31 October 2025

Abstract - Composite structures are extensively employed in various engineering applications to enhance strength and optimize overall performance through lightweight design. However, the complex manufacturing process of composite structures often introduces discontinuities like voids, holes, inclusions, cracks, delamination, and flaws. The interfacial cracks, particularly interlaminar debonding, interact with these discontinuities, posing a risk of failure in engineering components. Hence, studying Stress Intensity Factor (SIF) for various materials with interface cracks is important to avoid calamitous failures in various engineering applications. The stochastic approach is also applied by considering the random variables on material properties to obtain more accurate and optimized results.

Keywords - XFEM, COV, Mean, NISFs, Inclusion, Void, Interfacial crack.

1. Introduction

Dissimilar or composite structures find extensive use in numerous engineering applications due to their enhanced strength-to-weight ratio, which improves overall performance. However, the complex manufacturing process of composite structures introduces various discontinuities like holes, voids, inclusions, cracks, delamination, and flaws.

Among these, the interfacial cracks, specifically interlaminar debonding, interacting with the discontinuities, can possibly lead to failure in the different engineering components. Hence, it is important to study the Stress Intensity Factor (SIF) for various materials with interface cracks to prevent calamitous failures in various engineering applications.

In recent studies, researchers have examined Mode-I and the mixed-mode SIFs using diverse methodologies. Williams [1] explored the oscillatory behavior of interfacial cracks in dissimilar isotropic materials. Using the CVM, Sih et al. [2] produced a thorough equation to calculate stress, displacement, and SIF at the crack tip.. Dundurs [3] introduced parameters specific to orthogonal materials. Rice [4], along with Woo and Wang [5], expanded research on bimaterial interfacial crack plates. Additionally, Miyazaki et al. [6] investigated SIFs using the boundary element method for the aforementioned issues.

Chow et al. [7] present a finite element hybrid approach to determine displacements, strains, and the SIF near the interface crack-tip in various anisotropic media. Deng [8] performed asymptotic separation and delamination tests on composite panels. Lee et al. [9] investigated the SIF in the orthotropic materials under the dynamic loading conditions. Bjerkén and Persson [10] evaluated SIFs for various cases of bimaterial interfacial crack plates. Shukla et al. [11] analyzed the dynamic and static fracture failure at orthotropic and isotropic material interfaces using photo-elasticity. Sukumar et al. [12] presented that for cases of fractures at bimaterial interfaces, discontinuity enrichment functions were developed to determine the mixed-mode SIF.

Bordas et al. [13] introduced an object-oriented enriched finite element code by XFEM to solve different discontinuity problems. Menk and Bordas [14] proposed functions for enriching anisotropic and polycrystalline biomaterials using the XFEM. Ashari et al. [15] presented an enrichment function for orthotropic biomaterials and investigated various cases using the XFEM. Pathak et al. [16] evaluated several cases of bimaterial interfacial crack plates using the element-free Galerkin approach and the XFEM. Sharma et al. [17] investigated Mixed-Mode SIFs for the bimaterial of piezoelectric with a sub-interfacial crack by XFEM. The CVMMM was used by Gao et al. [18] to study the SIF for the crack in different materials. Hu et al. [19] assessed the crack

problem with a line interface crack and established a novel approach to studying different cases of an inclined crack in a bimaterial. Akhondzadeh et al. [20] provided stress singularity numerical models for XFEM multi-material contact challenges. Wang et al. [21] introduced higher-order enrichment functions that are material-dependent in XFEM to study interface crack issues that are curved and linear. Fan et al. [22] presented the DDM to evaluate bimaterial interface crack problems. Kumar et al. [23] evaluated the influence of interface cracks in cemented acetabular cups. Xiao et al. [24] introduced the single-region Boundary Element Method to analyze slant isotropic planes and interfaces of an isotropic bimaterial. Chai et al. [25] analyzed the interfacial elliptic crack SIFs and suggested the relative displacement basic functions for bimaterials.

The researchers have tackled the complexities of fracture mechanics, addressing different discontinuities such as cracks and interactions with inclusions/voids. Kaung et al. [26] utilized the Boundary Collocation Method to investigate crack emanation of holes in biomaterials. Sukumar et al. [27] presented enrichment functions of material interfaces in the XFEM using the level set method. Li et al. [28] evaluated Mode-I Stress Intensity Factors (SIFs) for cracks and inclusions by the Eshelby method. Belytschko et al. [29] presented XFEM's Volterra dislocation model for discontinuity problems: determining Peach-Koehler forces in complex scenarios. Shedbale et al. [30] presented the central crack issue with inclusions and holes for fatigue-life evaluation utilizing XFEM.

Natrajan et al. [31] and Sharma [32] studied various cracks with inclusion interactions to analyze SIFs by implementing the XFEM. Tafreshi [33] developed an algorithm to evaluate Jk-integrals for bimaterial interfacial cracks considering BECSS. Ebrahimi et al. [34] employed multi-pole methods (MPM) to simulate a crack with inclusion cases in brittle materials with separate crack dynamics. Yu et al. [35] assessed strong weak discontinuities by XFEM and using local approaches. Ismail et al. [36] examined SIF with numerous cracks at junctions in bimaterial plates. The Author presented curved interfacial modeling with element partitioning-free for the holes using XFEM.

Lal et al. [37] investigated an edge crack isotropic problem with voids and inclusions using various loading scenarios using the XFEM. The Author used XFEM to assess a variety of crack-void/inclusion interaction problems using Object-Oriented Programming (OOP). The Author explored interactions of various discontinuities in orthotropic plates through XFEM. Lal et al. [38] and Lal and Palekar [39] investigated laminate composite problems using stochastic XFEM with SOPT and MCS, considering random parameters. Khatri and Lal [40, 41] evaluated MMSIF, the corresponding Coefficients Of Variation (COV), and the crack propagation behavior for plates with the crack and hole subjected to

various loading conditions using stochastic XFEM with SOPT.

Wang et al. [45] present an improved peridynamics technique for simulating interfacial and sub-interfacial crack development in bimaterials, which successfully addresses singularity and mesh-dependency problems. Numerical data accurately match analytical and XFEM benchmarks, proving the model's ability to forecast crack initiation and propagation routes reliably. R Nikhil et al. [46] study uses a fracture model based on instability to forecast crack initiation in modified 9Cr-1Mo steel, taking into account the influence of void nucleation and growth. Ping Li et al. [47] present a novel strength-energy criterion for bimaterial interface crack propagation in order to increase prediction accuracy. Its efficiency over conventional methods is demonstrated by numerical and experimental validation. Maria A. and Vladislav [48] examine stress singularities in the generalized Comninou frictional contact model to gain insights into the behavior of interface cracks in anisotropic bimaterials. Palekar et al. [49] used the stochastic XFEM in their work to examine fracture in orthotropic laminated plates with double-edge cracks. It quantifies the effects of uncertainties in material and geometry on stress intensity factors and fracture behavior.

This literature review shows that researchers have devoted considerable attention to investigating various discontinuity interactions in composite materials using XFEM. They have employed diverse numerical methods to analyze Stress Intensity Factors (SIFs) considering interactions of cracks, voids, and inclusions in isotropic and orthotropic plates, as well as in bimaterials, addressing inclusions-voids with interface crack problems. This study aims to assess the Normalize Stress Intensity Factor (NSIF) using XFEM for an isotropic bimaterial problem involving interfacial edge cracks and void/inclusion interactions. A stochastic approach will also be applied, considering random variables for material properties. The primary focus of this study is to investigate NSIFs (K_I and K_{II}) and investigate the interaction of void/inclusions in interfacial edge crack isotropic bimaterials using XFEM, supplemented by a stochastic approach incorporating random material properties. The researcher has looked at the discontinuity issue with composite materials as well as a few applications of stochastic methods to analyzing SIF, but they have discovered very few combinations of them, discontinuities with bimaterial, and have used a stochastic approach.

2. Mathematical Formulation

The current study evaluates the NSIFs of the traction-free interface crack between two distinct media, taking into account the fundamental mathematical formulation of a bimaterial as reported by Asadpoure et al. [44] and Muhammadi S. [43]. In this study, the capricious bimaterial geometry is taken into consideration with different discontinuities such as void-inclusion, interfacial crack, under

traction force - f', global Cartesian coordinate - (X, Y), displacement - u, crack-tip located at (x_I, y_I) - the local Cartesian coordinate axis, and the local polar coordinate (r, θ) .

Figure 1 shows the crack-tip enclosed by Γ , the Γ -contour, and A -internal area with capricious boundary conditions.

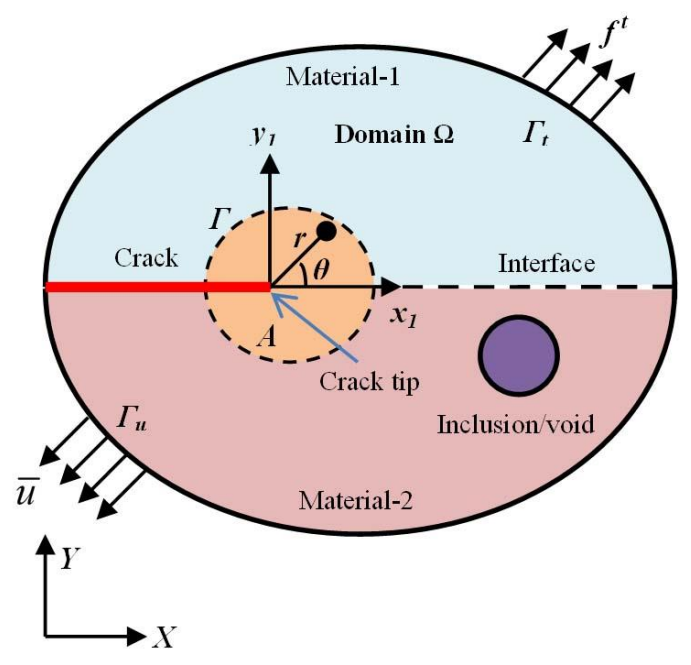


Fig. 1 Capricious bimaterial geometry of any kind with an interface fracture

2.1. An Isotropic Bimaterial Interface

Deng presented the fundamental asymptotic evaluation for a propagating and stationary interfacial edge crack in the isotropic bimaterial [8]. Sukumar et al. [12] presented the asymptotic solutions for an isotropic bimaterial edge crack by adopting the techniques of Rice [4], Mohammadi S. [43], and ignoring the effect of contact and crack propagation. Appendix -1 contains a detailed derivation of it.

2.2. XFEM Mathematical Formulation

This work takes into account those proposed by Mohammadi S. [43] and Asadpoure et al. [44] presented a general equation and boundary condition for the fracture field.

$$abla \sigma + f^q = 0$$
 in Ω (1)
 $\sigma n = f^t$ on Γ_t (2)
 $u = \bar{u}$ on Γ_u (3)
 $\sigma n = 0$ on Γ_c (4)

Where, $\Gamma_{\rm t}$ – external traction of the domain, $\Gamma_{\rm u}$ – displacement, $\Gamma_{\rm c}$ – the traction-free crack-boundary, σ -stress tensor, f- external traction, and body force.

XFEM can accurately predict the displacement at any position x inside the crack field by using the CFEM. And the enrichment hypothesis considers the effect of the crack tip and the crack surface,

$$u^{h}(x) = \sum_{j=1}^{CFEM} \mathbb{N}_{j}(x)u_{j} + \sum_{k=1}^{XFEMenrichment} \mathbb{N}_{k}(x)\Theta(x)a_{k}$$
 (5)

In CFEM, uj represents each node's regular degree of freedom and the discontinuous enrichment function, while Nj and Nk represent the discontinuity enrichment for *j* and *k*. Mohammadi S. [43] and Asadpoure et al. [44] regard each parameter of the XFEM enrichment function as provided.

According to Shedbale et al. [29] and Equation (5), void or inclusion for XFEM approximation is obtained for twodimensional media with varying discontinuities, such as cracks

$$u^{h}(x) = \sum_{j=1}^{n} \mathbb{N}_{j}(x)u_{j}$$

$$+ \sum_{k=1}^{cf} \mathbb{N}_{k}(x) \left(H(\xi(x)) \right)$$

$$- H(\xi(x_{k})) a_{k}$$

$$+ \sum_{l=1}^{ctp_{1}} \mathbb{N}_{l}(x) \left(\sum_{t=1}^{ctp_{1}} \left(\mathbb{Q}_{t}^{1}(x) - \mathbb{Q}_{t}^{1}(x_{l}) \right) \mathbb{C}_{l}^{t_{1}} \right) +$$

$$\sum_{m=1}^{ctp_{2}} \mathbb{N}_{m}(x) \left(\sum_{t=1}^{ctp_{2}} \left(\mathbb{Q}_{t}^{2}(x) - \mathbb{Q}_{t}^{2}(x_{m}) \right) \mathbb{C}_{m}^{t_{2}} \right)$$
(6)

$$+ \sum_{j=1}^{n} \mathbb{N}_{j}(x) \underbrace{\phi(x)d_{j}}_{\substack{j \in n_{incl} \\ n}}$$

$$+ \sum_{j=1}^{n} \mathbb{N}_{j}(x) \underbrace{[\psi(x) - \psi(x_{j})]\nu_{j}}_{\substack{j \in n_{void}}}$$

While cf - many nodes in the supported field for a crack surface, however not the crack tip, ctp_1 , ctp_2 - number of nodes in the affected field connected to crack-tips 1 and 2, a_k , $\mathbb{C}_l^{t_1}$, $\mathbb{C}_m^{t_2}$ - crack surface nodes and crack tip-1, 2 additional degree vector of the freedom, respectively. \mathbb{Q}_t^1 , \mathbb{Q}_t^2 - enrichment function of the crack tip 1, 2, respectively. ctp_1 or ctp_2 nodes represent the enriched function. The Heaviside function $H(\xi)$ enriches crack-supported field nodes and is not part of either the ctp_1 or ctp_2 .

Points that are located on the crack's positive side receive a +1, while all other points get -1, according to the $H(\xi(x))$ following definition:

$$H(\xi) = \begin{cases} +1 & \xi \in \Omega^+ \\ -1 & \xi \in \Omega^- \end{cases} \tag{7}$$

and,

 n_{incl} = the group of nodes whose components are removed through inclusion

void = the group of nodes whose components are removed through void

 d_j = nodal enriched dof accompanying with $\phi(x)$; where, (x) - level set function imitative,

$$\phi(x) = \pm \min \|x - x_{\Gamma}\| \quad (8)$$

where, $x\Gamma$ - the closest point from point x in the interface

 $vi = the \psi(x)$ - related nodal enhanced dof;

where $\psi(x)$ – Heavyside function, considered +1value for the nodes outside a hole, 0 value for the nodes inside a hole.

2.2.1. Isotropic Interface Enrichment Function

The following is how Sukumar et al. [12] developed the isotropic bimaterial,

$$\begin{bmatrix}
\Box_{i}^{j}(x)
\end{bmatrix}_{j=1,2} = \begin{bmatrix}
\sqrt{r}\cos(\overline{\omega})e^{-\omega\theta}\sin\frac{\theta}{2}, & \sqrt{r}\cos(\overline{\omega})e^{-\omega\theta}\cos\frac{\theta}{2}, \\
\sqrt{r}\cos(\overline{\omega})e^{\omega\theta}\sin\frac{\theta}{2}, & \sqrt{r}\cos(\overline{\omega})e^{\omega\theta}\cos\frac{\theta}{2}, \\
\sqrt{r}\sin(\overline{\omega})e^{-\omega\theta}\sin\frac{\theta}{2}, & \sqrt{r}\sin(\overline{\omega})e^{-\omega\theta}\cos\frac{\theta}{2}, \\
\sqrt{r}\sin(\overline{\omega})e^{\omega\theta}\sin\frac{\theta}{2}, & \sqrt{r}\sin(\overline{\omega})e^{\omega\theta}\cos\frac{\theta}{2}, \\
\sqrt{r}\sin(\overline{\omega})e^{\omega\theta}\sin\frac{\theta}{2}\sin\theta, & \sqrt{r}\cos(\overline{\omega})e^{\omega\theta}\cos\frac{\theta}{2}\sin\theta, \\
\sqrt{r}\sin(\overline{\omega})e^{\omega\theta}\sin\frac{\theta}{2}\sin\theta, & \sqrt{r}\sin(\overline{\omega})e^{\omega\theta}\cos\frac{\theta}{2}\sin\theta, \\
\sqrt{r}\sin(\overline{\omega})e^{\omega\theta}\sin\frac{\theta}{2}\sin\theta, & \sqrt{r}\sin(\overline{\omega})e^{\omega\theta}\cos\frac{\theta}{2}\sin\theta
\end{bmatrix}$$

Note that because the oscillatory index (ω) is determined using the characteristics of isotropic materials, Equation (9) cannot be applied to an orthotropic-bimaterial.

This is identical to the unidirectional orthotropic media's enrichment function that Asadpoure et al. presented. [44]:

$$\left[\mathbb{Q}_{l}(r,\theta)\right]_{l=1}^{4} = \left[\sqrt{r}\cos\frac{\theta_{1}}{2}\sqrt{g_{1}(\theta)}, \sqrt{r}\cos\frac{\theta_{2}}{2}\sqrt{g_{2}(\theta)}, \sqrt{r}\sin\frac{\theta_{1}}{2}\sqrt{g_{1}(\theta)}, \sqrt{r}\sin\frac{\theta_{2}}{2}\sqrt{g_{2}(\theta)}\right] \tag{10}$$

$$g_i(\theta) = \sqrt{\cos^2 \theta + \frac{\sin^2 \theta}{p_j^2}}, \quad j = 1, 2$$
 (11)

$$\theta_j = tg^{-1} \left(\frac{y}{p_j x} \right) = tg^{-1} \left(\frac{tg\theta}{p_j} \right)$$
 (12)

According to Mohammadi S. [43], the generic formulation in global form for an orthotropic material by the XFEM is defined.

$$K \times U = F \tag{13}$$

Where *K*, as defined by Shedbale et al. [29], is the overall stiffness matrix and F is the force vector,

$$K_{ij}^{e} = \begin{bmatrix} K_{ij}^{uu} & K_{ij}^{ua} & K_{ij}^{u^{\mathbb{C}}} & K_{ij}^{ud} & K_{ij}^{uv} \\ K_{ij}^{au} & K_{ij}^{aa} & K_{ij}^{a^{\mathbb{C}}} & K_{ij}^{ad} & K_{ij}^{av} \\ K_{ij}^{\mathbb{C}u} & K_{ij}^{\mathbb{C}a} & K_{ij}^{\mathbb{C}C} & K_{ij}^{\mathbb{C}d} & K_{ij}^{\mathbb{C}v} \\ K_{ij}^{du} & K_{ij}^{da} & K_{ij}^{d^{\mathbb{C}}} & K_{ij}^{dd} & K_{ij}^{dv} \\ K_{ij}^{vu} & K_{ij}^{va} & K_{ij}^{v^{\mathbb{C}}} & K_{ij}^{vd} & K_{ij}^{vv} \end{bmatrix}$$

$$(14)$$

$$F_i^e = \left\{ F_i^u F_i^a F_i^{\mathbb{C}_{t1}} F_i^{\mathbb{C}_{t2}} F_i^{\mathbb{C}_{t3}} F_i^{\mathbb{C}_{t4}} F_i^d F_i^v \right\}^T \tag{15}$$

U - nodal parameter vector

$$U = \{ ua\mathbb{C}_{t1}\mathbb{C}_{t2}\mathbb{C}_{t3}\mathbb{C}_{t4} \ d \ v \}^T$$
 (16)

Where

$$K_{ij}^{rs} = \int_{\Omega} e(B_i^r)^T DB_j^s d\Omega \qquad (r, s = u, a, C, d, v)$$
 (17)

$$f_i^u = \int_{\Gamma_t} \mathbb{N}_i f^t d\Gamma + \int_{\Omega^e} \mathbb{N}_i f^{C_t} d\Omega$$

$$f_i^a = \int_{\Gamma_t} \mathbb{N}_i H f^t d\Gamma + \int_{\Omega^e} \mathbb{N}_i H f^{\mathcal{C}_t} d\Omega \tag{18}$$

$$f_i^{C_{t\alpha}} = \int_{\Gamma_t} \mathbb{N}_i F_{\alpha} f^t d\Gamma + \int_{\Omega^e} \mathbb{N}_i F_{\alpha} f^{C_t} d\Omega , \qquad \alpha = 1, 2, ..., 8$$
(19)

$$f_i^d = \int_{\Gamma_t} \mathbb{N}_i \phi(x) \overline{t} d\Gamma + \int_{\Omega^e} \mathbb{N}_i \phi(x) \mathbb{C} d\Omega$$
 (20)

$$f_i^{v} = \int_{\Gamma_t} \mathbb{N}_i (\psi(x) - \psi(x_i)) \overline{t} d\Gamma + \int_{\Omega^e} \mathbb{N}_i (\psi(x) - \psi(x_i)) \mathbb{C} d\Omega$$
 (21)

Obtained matrix,

$$B_i^u = \begin{bmatrix} \mathbb{N}_{i,x_1} & 0\\ 0 & \mathbb{N}_{i,y_1}\\ \mathbb{N}_{i,y_1} & \mathbb{N}_{i,x_1} \end{bmatrix}$$
 (22)

$$B_i^a = \begin{bmatrix} (\mathbb{N}_i H)_{x_1} & 0\\ 0 & (\mathbb{N}_i H)_{y_1}\\ (\mathbb{N}_i H)_{y_1} & (\mathbb{N}_i H)_{x_1} \end{bmatrix}$$
(23)

$$B_i^{\mathbb{C}_t} = \begin{bmatrix} B_i^{\mathbb{C}_{t_1}} & B_i^{\mathbb{C}_{t_2}} & B_i^{\mathbb{C}_{t_3}} & B_i^{\mathbb{C}_{t_4}} \end{bmatrix} \tag{24}$$

$$B_{i}^{Ct_{\alpha}} = \begin{bmatrix} (N_{i}F_{\alpha})_{x_{1}} & 0\\ 0 & (N_{i}F_{\alpha})_{y_{1}}\\ (N_{i}F_{\alpha})_{y_{1}} & (N_{i}F_{\alpha})_{x_{1}} \end{bmatrix}, \qquad \alpha = 1,2,...,8 \quad (25)$$

$$B_i^d = \begin{bmatrix} (\mathbb{N}_i \phi(x))_{,x} & 0\\ 0 & (\mathbb{N}_i \phi(x))_{,y}\\ (\mathbb{N}_i \phi(x))_{,y} & (\mathbb{N}_i \phi(x))_{,x} \end{bmatrix}_{3\times8} (26)$$

$$B_i^v = \begin{bmatrix} \left(\mathbb{N}_i(\psi(x) - \psi(x_i)) \right)_{,x} & 0 \\ 0 & \left(\mathbb{N}_i(\psi(x) - \psi(x_i)) \right)_{,y} \\ \left(\mathbb{N}_i(\psi(x) - \psi(x_i)) \right)_{,y} & \left(\mathbb{N}_i(\psi(x) - \psi(x_i)) \right)_{,x} \end{bmatrix}_{3 \times 8}$$

$$(27)$$

2.3. NMMSIF Mathematical Formulation

Similar to Mohammadi S. [43], this study employs the integral domain technique to model a fracture in an orthotropic (homogeneous) material with integral. Evaluate the NMMSIFs K_I and K_{II} ,

$$J = \int_{A} \left(\sigma_{ij} \frac{\partial u_{j}}{\partial x} - W_{st} \Delta_{1j} \right) \frac{\partial q}{\partial x_{j}} dA$$
 (28)

The defined domain's real and auxiliary conditions, taking into account two equality criteria. The J - integral, J^s (through the effect of both circumstances), is determined. Furthermore, as seen in Figure 1, from the crack tip, where q=1, to the outer boundary of Γ , where q=0, the value of q changes continuously, see Appendix 1 for more. All additional displacement and stress fields are included in one.

By combining the auxiliary and real conditions, the J-integral is calculated like this:

$$J^S = J^{Act} + J^{Aux} + M (29)$$

Here, M found,

$$M = \int_{A} \left[\sigma_{ij} \frac{\partial u_{i}^{aux}}{\partial x} + \sigma_{ij}^{aux} \frac{\partial u_{i}}{\partial x} - W_{st}^{m} \Delta_{1j} \right] \frac{\partial q}{\partial x_{j}} dA$$
 (30)

or linear elastic conditions,

$$W_{st}^{\ m} = \frac{\sigma_{ij}\varepsilon_{ij}^{aux} + \sigma_{ij}^{aux}\varepsilon_{ij}}{2}$$
 (31)

The crack tip, where FE analysis is becoming more precise, shares a similar route freedom as the original J-integral and is used to calculate the M-integral.

To calculate the SIF, Chow et al. [7] presented a relationship for subordinating the SIF to - integral. *M*-integral orthotropic bimaterial medium:

$$K_i = 2\sum_{m=1}^{2} U_{im} M(u, u^{aux(m)}), \quad i = 1, 2$$
 (32)

The SIFs K_I and K_{II} are found by using two conditions $(K_I^{aux}=1,\ K_{II}^{aux}=0)$, $(K_{II}^{aux}=1,\ K_I^{aux}=0)$ respectively, and

$$U = [(L_1^{-1} + L_2^{-1})^{-1}(I + \beta^2)]^{-1}$$
 (33)

$$\beta = (L_1^{-1} + L_2^{-1})^{-1} (S_1 L_1^{-1} - S_2 L_2^{-1})^{-1} \ \, (34)$$

As Barnett and Lothe (1973) explain, the subscripts 1 and 2 represent the top and bottom media, respectively, whereas S and L represent the corresponding 2×2 . Deng [8] outlines the precise conditions for when a genuine Barnett Lothe tensor has no zero components in an orthotropic medium.

$$S_{21} = \left[\frac{c_{66}(\sqrt{c_{11}c_{22}} - c_{12})}{c_{22}(c_{12} + 2c_{66} + \sqrt{c_{11}c_{22}})} \right]^{\frac{1}{2}}, \quad S_{12} = -\sqrt{\frac{c_{22}}{c_{11}}} S_{21}$$
(35)

$$L_{11} = (C_{12} + \sqrt{C_{11}C_{22}})S_{21}, \quad L_{22} = -\sqrt{\frac{C_{22}}{C_{11}}}L_{11}$$
 (36)

Where C_{ij} is the abbreviated version of the 4th order elastic constant tensor $C_{ijkl} = S_{ijk}^{-1}$, each layer's S and L components are identified separately.

2.4. FOPT and SOPT by implementing the XFEM

Stochastic XFEM extends deterministic XFEM by incorporating arbitrariness in various properties, including material, geometry, and loadings, through the Second-Order Perturbation Technique (SOPT) by expansion of the Taylor series. Compared to other stochastic methods, perturbation techniques are notably more efficient. In the engineering issues involving the random variables, the parameters' Coefficients of Variation (COV) are typically slight [40, 41]. In this study, both the static and random components of MMSIFs (mixed–mode intensity factor) are expressed as functions of the random and static components or the first and for 1st and 2nd modes of SIF, respectively. This relationship can be illustrated as:

$$K = f(K_n), n = \begin{cases} I & for \operatorname{mod} e - I \\ II & for \operatorname{mod} e - II \end{cases}$$
(37)

The MMSIFs K_n value is subject to various random variables e_i , independent or dependent on each other, with the mean μ_{e_i} standard deviation σ_{e_i} . In addition, the MMSIFs can be displayed using random variables K_I and K_{II} as:

If, n = I and n = II,

$$K_I = K_I(e_i) , K_{II} = K_{II}(e_i)$$
 (38)

Currently, the perturbation method or Taylor series expansion method is utilized to introduce randomness into the system as follows:

$$K = K_n(\mu_{e_i}) + \sum_{i=1}^N e_i \frac{\partial K_n}{\partial e_i} + \frac{1}{2} \sum_{i=1}^N \sum_{j=1}^N e_i e_j \frac{\partial^2 K_n}{\partial e_i \partial e_j}$$
(39)
Where e_i , $e_j(i, j = 1, 2, ..., N)$ - random variables are denoted with $(x_i - \mu_{e_i})$ and $(x_j - \mu_{e_j})$, respectively, $K_n(\mu_{e_i})$ - mean values of the MMSIFs using the input variable..

The
$$E[K'_n]$$
 mean of the first order of K is represented by, $E[K'_n] \approx K_n(\mu_{e_i})$ (40)

Now, the 1^{st} order variance of K is indicated by,

$$Var(K') \approx \sum_{i=1}^{n} \sum_{j=1}^{n} \frac{\partial K_n}{\partial e_i} \frac{\partial K_n}{\partial e_j} COV[e_i, e_j]$$
 (41)

in which n - total quantity of the random variable and

$$COV[e_i, e_i] = [A][A'], \tag{42}$$

$$[A] = \begin{bmatrix} \sigma_{e_1}^2 & COV(e_1, e_2) & \dots & COV(e_1, e_i) \\ COV(e_2, e_1) & \sigma_{e_2}^2 & \dots & COV(e_2, e_i) \\ \dots & \dots & \dots & \dots \\ COV(e_i, e_2) & COV(e_i, e_2) & \dots & \sigma_{e_i}^2 \end{bmatrix} 43)$$

And
$$[A'] = \begin{bmatrix} 1 & \rho_{e_1,e_2} & \dots & \rho_{e_1,e_i} \\ \rho_{e_2,e_1} & 1 & \dots & \rho_{e_2,e_i} \\ \dots & \dots & \dots & \dots \\ \rho_{e_i,e_1} & \rho_{e_i,e_1} & \dots & 1 \end{bmatrix}$$

$$(44)$$

Where $\begin{bmatrix} A \end{bmatrix}$ and $\begin{bmatrix} A \end{bmatrix}$ a are the random variables' associated coefficient matrices and standard deviation, respectively. Furthermore,

$$\sigma_{e_1}, \ \sigma_{e_2}, \dots, \sigma_{e_i} = COV(e_i, e_j) \ K_n(\mu_{e_1}, \ \mu_{e_2}, \dots, \mu_{e_i}) \quad \text{and}$$

$$\rho_{e_i, e_j} = \frac{COV(e_i, e_j)}{\sigma_{e_i} \cdot \sigma_{e_j}}$$

$$(45)$$

Where, $COV(e_i, e_j)$ for uncorrelated random variables, the relationship between the random variable and its values is set to be zero. On the other hand, ρ_{e_i,e_j} for the interrelated random variable, any value of the COC- coefficient of correlation can be assumed.

Using a higher-order term in the Taylor series expansion of $K_n(e_i)$ can help get a better estimate of the average and spread of MMSIFs K. The second-order mean of MMSIFs K is obtained by using the SOPT method, which is a second-order perturbation technique:

$$E[K''] = K_n(\mu_{e_i}) + \frac{1}{2}Var\{K_n\}$$
 (46)

And the response's $E[K_n'']$ matching second-order variance matrix, which is displayed as follows, is equivalent to the 1st order matrix of variance provided in Equation (40):

$$Var\{K''\} = Var\{K'\} \tag{47}$$

The information about the $3^{\rm rd}$ and $4^{\rm th}$ moments of this is needed for the estimation of the $2^{\rm nd}$ order variance. Nevertheless, this kind of information is typically unavailable. For the majority of real-world engineering applications, using the $2^{\rm nd}$ order mean and $1^{\rm st}$ order variance is seen to be sufficient. The MMSIFs' K_I and K_{II} mean and variance are computed in this manner. Standard deviation (SD) can also be computed as follows:

Standard Deviation (SD) = $\sqrt{\text{Variance}}$ Moreover, the Coefficient of Variance (COV) is:

COV = SD/Mean

Because of its intricate derivations and expressions, the SOPT is challenging to integrate. Therefore, the Finite Difference Method (FDM) can be used to calculate the first-order sensitivity with respect to specified random variables $\left\{ \frac{\partial K_n}{\partial e_i R} \right\}$. FDM is used to calculate the first-order sensitivity as follows:

$$\frac{\partial K_n}{\partial e_i} = \frac{K_n(e_i + \delta e_i) - K_n(e_i - \delta e_i)}{2\delta e_i} \tag{48}$$
 Where ∂e_i is a deviation from the mean values of the

Where ∂e_i is a deviation from the mean values of the random variables' coefficient of variation, or the design parameter. Mean-centered SOPT is used to analyze the mean values as well as the standard deviation. The perturbation technique's shortcomings are (a) for the solution to be obtained up to the required precision, the variability in randomness should remain moderate, i.e., the Coefficient of Variance (COV) < 0.2, where COV represents the relative amount of uncertainty/ randomness. (b) Because the partial derivatives $\frac{\partial K_n}{\partial e_i} \frac{\partial^2 K_n}{\partial e_i \partial e_j}$ must be calculated, the approach has a higher computing cost, particularly in large stochastic dimensions.

3. Results and Discussion

3.1. The Crack Plate at the Bimaterial Interface is under an Uniaxial Tensile Force

Numerical studies are carried out on bimaterial interface edge crack scenarios under uniaxial tensile loads, both with and without void/inclusion, using XFEM. The geometric dimensions, following Pathak et al. [16], are set at 200 mm \times 100 mm (length \times width) for all interfacial edge crack cases.

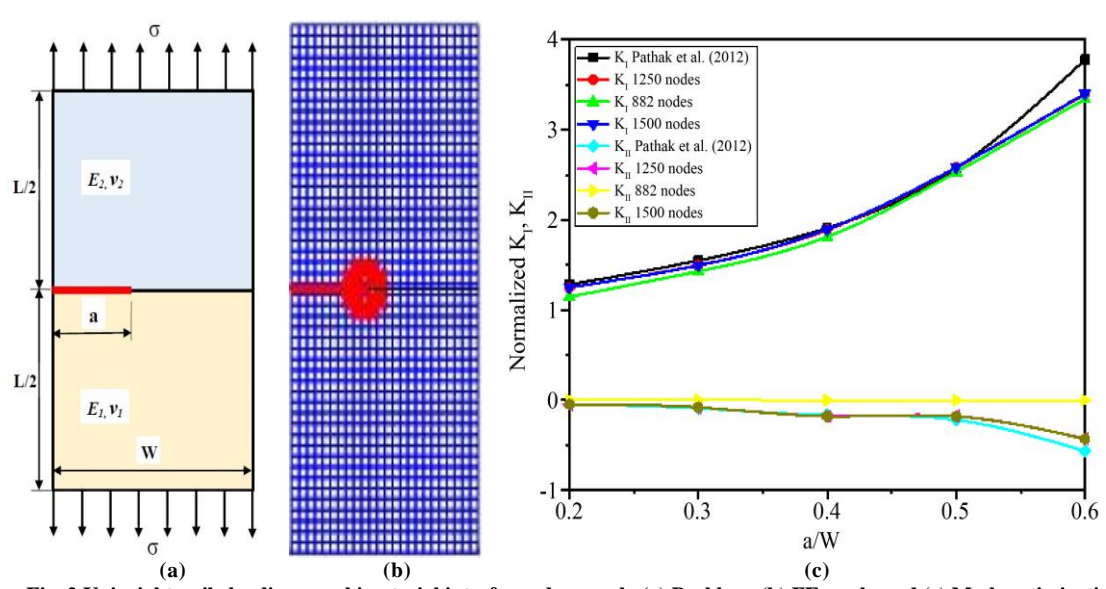
The XFEM is used to implement 1176 elements and 1250 nodes in total, with Q4-elements being used for numerical simulations in all scenarios within the MATLAB code. Each case study assesses plain strain conditions and evaluates the NSIF - K_I and K_{II} accordingly.

$$K_I = \overline{K}_I / \sigma \sqrt{\pi \cdot a}$$
 and $K_{II} = \overline{K}_{II} / \sigma \sqrt{\pi \cdot a}$ with uniaxial-tensile stress

3.1.1. Problem for the Validation

The validation study uses XFEM to analyze a bimaterial interface edge-cracked plate under uniaxial tensile stress. The geometry remains consistent with the dimensions mentioned earlier. This work sets an uniaxial tensile stress to $\sigma=1$ MPa. Both materials have the same Poisson's ratio ($\nu=\nu_1=\nu_2$), set to 0.3.

The ratio of Young's modulus E_2/E_1 is taken as 2 and 100, where $E_1 = 205.8$ MPa, following the parameters used by Pathak et al. [16]. For the various ratios (a/W = 0.2, 0.3, 0.4, 0.5, and 0.6) of an interface edge crack length, NSIFs K_I and K_{II} are calculated and compared to Pathak et al. [16] findings. Figure 2 shows a problem domain, FE meshing for a bimaterial interface edge crack problem.



 $Fig.\ 2\ Uniaxial\ tensile\ loading\ on\ a\ bimaterial\ interface\ edge-crack, (a)\ Problem, (b)\ FE\ mesh,\ and\ (c)\ Mesh\ optimization.$

The study of mesh optimization depicted in Figure 2(c) reveals that, in comparison to the results obtained by Pathak et al. [16], the NSIF values are lower when using 882 nodes (21 x 42), but closer to the results obtained with 1250 nodes (25 x 50). Additionally, the NSIFs results obtained with 1250 and 1500 nodes exhibit a very similar trend. Therefore, for this

study, 1250 nodes are considered the optimal mesh density. The NSIFs K_I and K_{II} are found for the various ratios (a/W) of crack length with $E_2/E_1 = 2$ and compared with Pathak et al. [16] results, as shown in Figure 3(a). It has been noted that the results obtained closely match those of Pathak et al. [16]. Similarly, NSIFs K_I and K_{II} are found for the different a/W

crack length ratio with $E_2/E_1 = 100$ and compared with Pathak et al.'s [16] results, as illustrated in Figure 3(b). Again, the results are found to be very close to those obtained by Pathak

et al. [16]. Figure 3 shows that NSIFs K_I increase while NSIFs K_{II} decrease by increasing a/W = 0.2, 0.3..., 0.6 subject to an uniaxial tensile load.

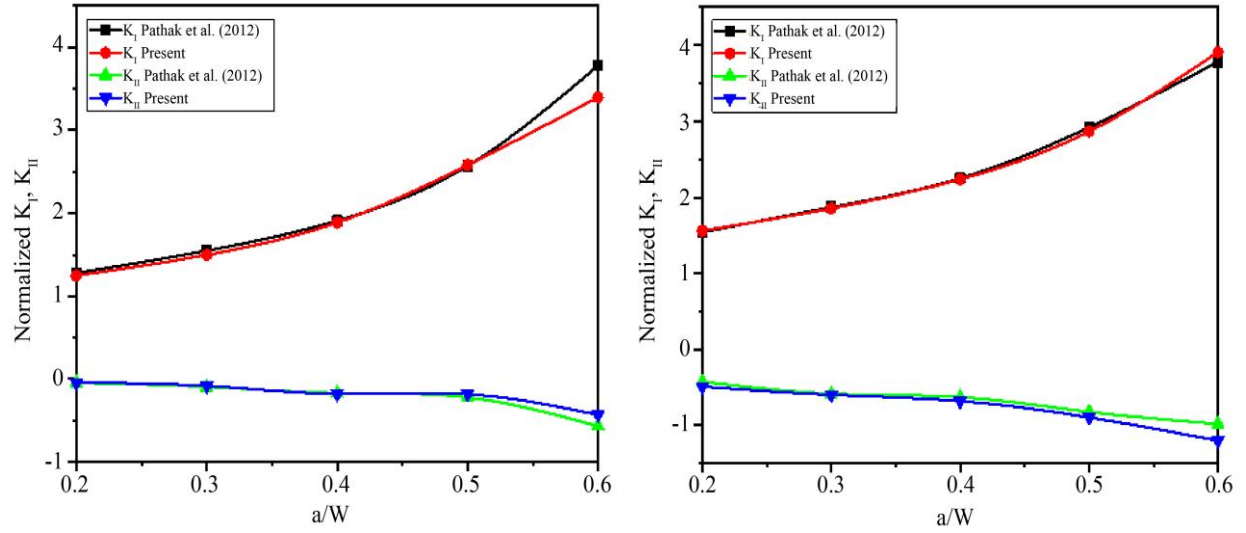


Fig. 3 NSIFs K_I and K_{II} for a bimaterial interface edge-crack subject to uniaxial tensile load, (a) $E_2/E_1 = 2$, and (b) $E_2/E_1 = 100$.

The XFEM solution approach employed in Pathak et al. [16] literature review is employed in this work. As depicted in Figure 3, the results obtained in the present study show improvement ranging from 7% to 9% for crack length ratios (a/W) of 0.2-0.6 by implementing the Matlab analytical code. Particularly for a/W= 0.6, significantly amended results were found, indicating a notable difference compared to the literature results.

Pathak et al. [16] compared their findings with those obtained using the EFGM (Element Free Galerkin Method) and results from other researchers. In the present work, the XFEM was used, and the results were compared specifically with the XFEM results found by Pathak et al. [16].

3.1.2. The Void/Inclusion is aligned with a Bimaterial Interface Edge-Crack

With the bimaterial interface edge-crack in alignment with a circular void/inclusion, a system is exposed to a uniaxial tensile force using XFEM. The radius of the void/inclusion is 0.10W, where W is the plate's width. When $E_2/E_1=2$, the material properties for the inclusion are $E_2\times 10^3$ MPa, and when $E_2/E_1=100$, they are $E_2\times 10^5$ MPa. As seen in Figure 4, the void or inclusion is positioned at L/2 and W/4.

The characteristics of a material, the uniaxial tensile stress, and different interface edge-crack lengths – a/W align with those employed in a validation problem study to assess the NSIFs K_I and K_{II} . This study aims to examine the impact of an inclusion or void oriented parallel to the interfacial edge crack in situations where $E_2/E_1 = 2$ and = 100

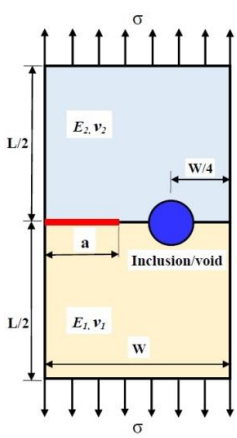


Fig. 4 The geometry of an inclusion or void that is aligned with a bimaterial interface edge crack under uniaxial tensile load

Figure 5(a) shows that NSIF KI increases to 16% when considered a void and decreases to 12% when considering that inclusion. Conversely, the NSIF K_{II} decreases nearly 2.1 times to the void, increasing by nearly 2.8 times to inclusion, as the crack length ratio (a/W) increases from 0.2 to 0.6 for $E_2/E_1 = 2$. Similarly, in Figure 5(b), with an inclusion, the NSIF K_I is seen to fall to about 20%, while with a void, it rises to about 13%. The NSIF, on the other hand, is seen to behave differently. Over the same a/W range, the NSIF K_{II} drops close to 2.3 times to void, and increases close to 2.3 times to the inclusion. Except for when $E_2/E_1 = 100$, it is between 0.2 and 0.6. Notably, the NSIF K_{II} increases with void and decreases with inclusion, whereas the NSIF K_{II} exhibits the opposite trend when compared to the scenario without a void or inclusion. This variation is more pronounced at a/W = 0.5 and

0.7. Furthermore, the disparity between the results of the three cases is more pronounced for a/W=0.6 compared to a/W=0.2, primarily due to the fact that the position of the void or

inclusion remains the same for all three cases, and as the crack length increases, the crack tip moves closer to the void/inclusion, amplifying its influence.

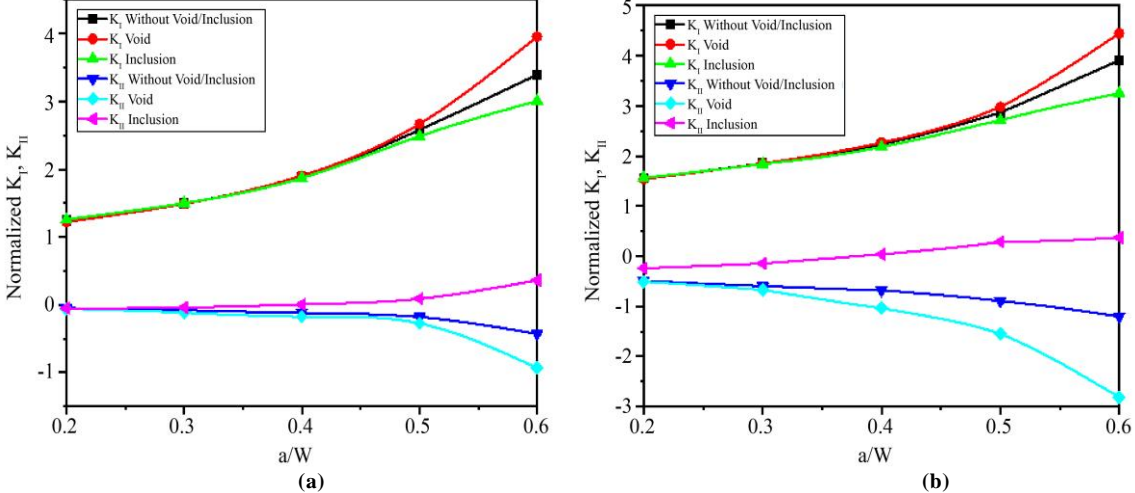


Fig. 5 When under uniaxial tensile load, the bimaterial interface edge-crack was aligned with the \overline{KI} and \overline{KII} of the void/inclusion NSIFs, (a) E2/E1 = 2, (b) E2/E1 = 100

3.2. Stochastic Analysis of Void/Inclusion is Aligned at a Bimaterial Interface with an Edge Crack

In this scenario, Stochastic XFEM analysis is used to examine an edge-crack under uniaxial tensile stress in the form of a circular void or inclusion aligned with a bimaterial interface. A void or an inclusion has a radius of 0.10W, and the inclusion material has a Young's modulus of $E_2 \times 10^3$ MPa for the case where $E_2/E_1 = 2$. The location of a void or an inclusion is set at L/2 and W/4, as depicted in Figure 6. The characteristics of a material, the uniaxial tensile stress, and different interface edge-crack lengths (a/W) remain consistent with those used in the validation problem study to analyze the Coefficient of Variation (COV) and the mean of NSIFs K_I and K_{II} using XFEM and SOPT. This investigation aims to assess the effect of a single void or an inclusion in line with the interface edge-crack of the case where $E_2/E_1 = 2$.

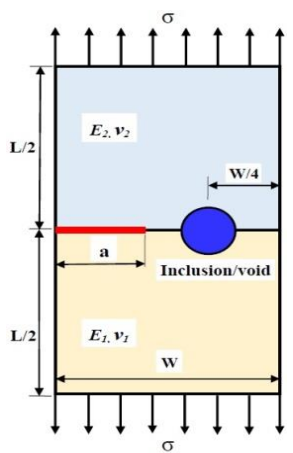


Fig. 6 The geometry of a void or an inclusion aligned to an abimaterial interface edge crack under the uniaxial tensile load

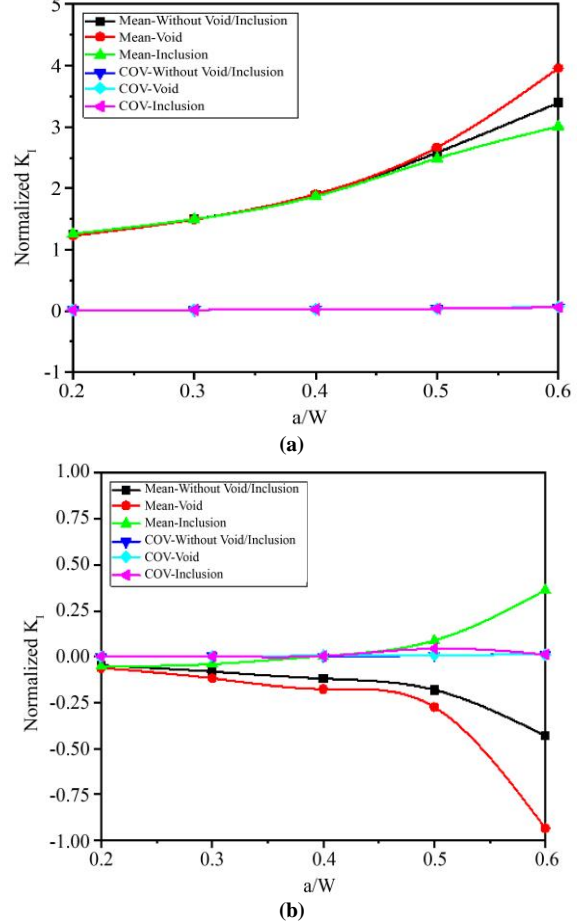


Fig. 7 NSIFs KI and KII for a crack at the edge of a bimaterial interface, either in a void or an inclusion, when the material is subjected to uniaxial tensile stress, (a) E2/E1 = 2, (b) E2/E1 = 100.

This study investigates the impact of random system parameters on Young's modulus (E1). The fundamental system random variable (bi) utilized for bimaterial interfacial edge crack plates is defined as follows: $b_I = E_{11}$. Figure 7 and Table 1 depict the influence of the random variable E_1 on the Coefficient of Variation (COV) and the mean of NSIFs. It is investigated that the mean values of NSIF K_I increase by 16% when considering a void, and decrease to 12% when

considering an inclusion. Conversely, the mean value of NSIF K_{II} decreases to 2.1 times to void and increases to 2.8 times to inclusion as the crack length ratio (a/W) increases from 0.2 to 0.6 for $E_2/E_1 = 2$. Notably, NSIF K_I increases with void and decreases with inclusion, whereas NSIF K_{II} exhibits the opposite trend compared to the scenario without a void or an inclusion. This variance is more pronounced at a/W = 0.5 and 0.6.

bimaterial plate with an edge crack at the interface when the plate is under a uniaxial tensile load?											
			Without	Void	Inclusion						

RV	a/W	NSIF	Without Void/Inclusion		Void		Inclusion	
			Mean	COV	Mean	COV	Mean	COV
	0.2	K_I	1.2469	0.0141	1.2251	0.0139	1.2585	0.0138
		K_{II}	-0.0467	0.0004	-0.0609	0.0010	-0.0518	0.0017
	0.3	K_I	1.4977	0.0189	1.4902	0.0186	1.4992	0.0187
		K_{II}	-0.0808	0.0028	-0.1170	0.0033	-0.0396	0.0023
E_I	0.4	K_I	1.8893	0.0265	1.9041	0.0263	1.8697	0.0265
E1		K_{II}	-0.1190	0.0009	-0.1760	0.0057	0.0046	0.0038
	0.5	K_I	2.5816	0.0377	2.6680	0.0371	2.4871	0.0372
		K_{II}	-0.1800	0.0076	-0.2740	0.0095	0.0885	0.0446
	0.6	K_I	3.3947	0.0613	3.9568	0.0688	3.0074	0.0603
		K_{II}	-0.4300	0.0140	-0.9335	0.0121	0.3626	0.0122

4. Conclusion

The NSIF K_I exhibits a notable increase in the presence of a void and a decrease when an inclusion is introduced, whereas NSIF K_{II} shows the opposite behavior, decreasing with a void and increasing with an inclusion. These variations are particularly pronounced in the case of an interface edge crack at normalized crack lengths of a/W = 0.5 and 0.6, highlighting the sensitivity of the SIFs to these geometrical and material changes. When a stochastic approach is employed, the mean values of NSIF K_I and K_{II} maintain a consistent trend, and their Coefficients of Variation (COVs) are observed to be close to zero, indicating minimal variability and a high degree of reliability in the results under the given conditions. To enhance the understanding of these behaviors, further investigations should focus on a wider range of crack

geometries, material combinations, and loading conditions. Incorporating three-dimensional models and experimental validation would strengthen the reliability of these findings. The study is limited to specific interface configurations and assumes idealized conditions, which may not fully capture complexities in real-world applications. The stochastic approach, while effective, may require refinement to account for nonlinear interactions and higher-order effects.

The findings offer insights into how cracks behave in uncertain conditions, which helps with material selection, structural design, and reliability evaluation. In engineering applications, this method promotes composite and bimaterial systems that are more secure, resilient, and resistant to damage.

References

- [1] M.L. Williams, "The Stresses Around a Fault or Crack in Dissimilar Media," *Bulletin of the Seismological Society of America*, vol. 49, no. 2, pp. 199-204, 1959. [CrossRef] [Google Scholar] [Publisher Link]
- [2] G.C. Sih, P.C. Paris, and G.R. Irwin, "On Cracks in Rectilinearly Anisotropic Bodies," *International Journal of Fracture Mechanics*, vol. 1, pp. 189-203, 1965. [CrossRef] [Google Scholar] [Publisher Link]
- [3] J. Dundurs, "Discussion: "Edge-Bonded Dissimilar Orthogonal Elastic Wedges Under Normal and Shear Loading," *Journal of Applied Mechanics*, vol. 36, no. 3, pp. 650-652, 1969. [CrossRef] [Google Scholar] [Publisher Link]
- [4] J.R. Rice, "Elastic Fracture Mechanics Concepts for Interfacial Cracks," *Journal of Applied Mechanics*, vol. 55, no. 1, pp. 98-103, 1988. [CrossRef] [Google Scholar] [Publisher Link]
- [5] C.W. Woo, and Y.H. Wano, "Analysis of an Edge Crack in a Finite Bi-Material Plate," *Engineering Fracture Mechanics*, vol. 42, no. 2, pp. 289-297, 1992. [CrossRef] [Google Scholar] [Publisher Link]

- [6] Noriyuki Miyazaki et al., "Stress Intensity Factor Analysis of Interface Crack using Boundary Element Method: Application of Virtual Crack Extension Method," *JSME International Journal, Series A: Mechanics and Material Engineering*, vol. 36, no. 1, pp. 36-42, 1993. [CrossRef] [Google Scholar] [Publisher Link]
- [7] W.T. Chow, H.G. Beom, and S.N. Atluri, "Calculation of Stress Intensity Factors for an Interfacial Crack between Dissimilar Anisotropic Media, using a Hybrid Element Method and the Mutual Integral," *Computational Mechanics*, vol. 15, pp. 546-557, 1995. [CrossRef] [Google Scholar] [Publisher Link]
- [8] Xiaomin Deng, "Mechanics of Debonding and Delamination in Composites: Asymptotic Studies," *Composites Engineering*, vol. 5, no. 10-11, pp. 1299-1315, 1995. [CrossRef] [Google Scholar] [Publisher Link]
- [9] Kwang-Ho Lee, Jai-Sug Hawong, and Sun-Ho Choi, "Dynamic Stress Intensity Factors KI, KII and Dynamic Crack Propagation Characteristics of Orthotropic Material," *Engineering Fracture Mechanics*, vol. 53, no. 1, pp. 119-140, 1996. [CrossRef] [Google Scholar] [Publisher Link]
- [10] Christina Bjerkén, and Christer Persson, "A Numerical Method for Calculating Stress Intensity Factors for Interface Cracks in Biomaterials," *Engineering Fracture Mechanics*, vol. 68, no. 2, pp. 235-246, 2001. [CrossRef] [Google Scholar] [Publisher Link]
- [11] Arun Shukla et al., "Photoelastic Investigation of Interfacial Fracture between Orthotropic and Isotropic Materials," *Optic and Lasers in Engineering*, vol. 40, no. 4, pp. 307-324, 2003. [CrossRef] [Google Scholar] [Publisher Link]
- [12] N. Sukumar et al., "Partition of Unity Enrichment for Bimaterial Interface Cracks," *International Journal for Numerical Methods in Engineering*, vol. 59, pp. 1075-1102, 2004. [CrossRef] [Google Scholar] [Publisher Link]
- [13] Stéphane Bordas et al., "An Extended Finite Element Library," *International Journal for Numerical Methods in Engineering*, vol. 71, no. 6, pp. 703-732, 2007. [CrossRef] [Google Scholar] [Publisher Link]
- [14] Alexander Menk, and Stéphane P.A. Bordas, "Numerically Determined Enrichment Functions for the Extended Finite Element Method and Applications to Bi-Material Anisotropic Fracture and Polycrystals," *International Journal for Numerical Methods in Engineering*, vol. 83, no. 7, pp. 805-828, 2010. [CrossRef] [Google Scholar] [Publisher Link]
- [15] S. Esna Ashari, and S. Mohammadi, "Delamination Analysis of Composites by New Orthotropic Bimaterial Extended Finite Element Method," *International Journal for Numerical Methods in Engineering*, vol. 86, no. 13, pp. 1507-1543, 2011. [CrossRef] [Google Scholar] [Publisher Link]
- [16] Himanshu Pathak, Akhilendra Singh, and Indra Vir Singh "Numerical Simulation of Bi-Material Interfacial Cracks using EFGM and XFEM," *International Journal of Mechanics and Materials in Design*, vol. 8, pp. 9-36, 2012. [CrossRef] [Google Scholar] [Publisher Link]
- [17] K. Sharma et al., "Analysis of a Subinterface Crack in Piezoelectric Bimaterials with the Extended Finite Element Method," *Engineering Fracture Mechanics*, vol. 104, pp. 114-139, 2013. [CrossRef] [Google Scholar] [Publisher Link]
- [18] Hongfen Gao, and Gaofeng Wei, "Stress Intensity Factor for Interface Cracks in Bimaterials Using Complex Variable Meshless Manifold Methods," *Mathematical Problems in Engineering*, vol. 2014, no. 1, pp. 1-8, 2014. [CrossRef] [Google Scholar] [Publisher Link]
- [19] X.F. Hu, J.N. Wang, and W.A. Yao, "A Size Independent Enriched Finite Element for the Modeling of Bimaterial Interface Cracks," *Computers & Structures*, vol. 172, pp. 1-10, 2016. [CrossRef] [Google Scholar] [Publisher Link]
- [20] Sh. Akhondzadeh, A.R. Khoei, and P. Broumand, "An Efficient Enrichment Strategy for Modeling Stress Singularities in Isotropic Composite Materials with X-FEM Technique," *Engineering Fracture Mechanics*, vol. 169, pp. 201-225, 2017. [CrossRef] [Google Scholar] [Publisher Link]
- [21] Yongxiang Wang et al., "XFEM with High-Order Material-Dependent Enrichment Functions for Stress Intensity Factors Calculation of Interface Cracks using Irwin's Crack Closure Integral," *Engineering Fracture Mechanics*, vol. 178, pp. 148-168, 2017. [CrossRef] [Google Scholar] [Publisher Link]
- [22] Fan CuiYing et al., "Fundamental Solutions and Analysis of the Interface Crack for Two-Dimensional Decagonal Quasicrystal Bimaterial via the Displacement Discontinuity Method," *Engineering Analysis with Boundary Elements*, vol. 106, pp. 462-472, 2019. [CrossRef] [Google Scholar] [Publisher Link]
- [23] Ajay Kumar, Rajesh Ghosh, and Rajeev Kumar, "Effects of Interfacial Crack and Implant Material on Mixed-Mode Stress Intensity Factor and Prediction of Interface Failure of Cemented Acetabular Cup," *Journal of Biomedical Materials Research Part B: Applied Biomaterials*, vol. 108, no. 5, pp. 1844-1856, 2019. [CrossRef] [Google Scholar] [Publisher Link]
- [24] Sha Xiao, Zhongqi Quentin Yue, and Hongtian Xiao, "Boundary Element Analysis of Transversely Isotropic Bi-Material Halfspaces with Inclined Planes of Isotropy and Interfaces," *International Journal for Numerical and Analytical Methods in Geomechanics*, vol. 43, no. 17, pp. 2599-2627, 2019. [CrossRef] [Google Scholar] [Publisher Link]
- [25] Hao Chai, Jun Lv, and Yumei Bao, "Numerical Solutions of Hypersingular Integral Equations for Stress Intensity Factors of Planar Embedded Interface Cracks and their Correlations with Bimaterial Parameters," *International Journal of Solids and Structures*, vol. 202, pp. 184-194, 2020. [CrossRef] [Google Scholar] [Publisher Link]
- [26] J.S. Kuang, and Y.H. Wang, "Bimaterial Interface Cracks Originating from Holes," *Mechanics Research Communications*, vol. 22, no. 6, pp. 577-582, 1995. [CrossRef] [Google Scholar] [Publisher Link]

- [27] N. Sukumar et al., "Modeling Holes and Inclusions by Level Sets in the Extended Finite-Element Method," *Computer Methods in Applied Mechanics and Engineering*, vol. 190, no. 46-47, pp. 6183-6200, 2001. [CrossRef] [Google Scholar] [Publisher Link]
- [28] Ted Belytschko, and Robert Gracie, "On XFEM Applications to Dislocations and Interfaces," *International Journal of Plasticity*, vol. 23, no. 10-11, pp. 1721-1738, 2007. [CrossRef] [Google Scholar] [Publisher Link]
- [29] A.S. Shedbale, I.V. Singh, and B.K. Mishra, "Nonlinear Simulation of an Embedded Crack in the Presence of Holes and Inclusions by XFEM," *Procedia Engineering*, vol. 64, pp. 642-651, 2013. [CrossRef] [Google Scholar] [Publisher Link]
- [30] S. Natarajan et al., "Numerical Analysis of the Inclusion-Crack Interaction by the Extended Finite Element Method," *International Journal for Computational Methods in Engineering Science and Mechanics*, vol. 15, no. 1, pp. 26-32, 2014. [CrossRef] [Google Scholar] [Publisher Link]
- [31] K. Sharma, "Crack Interaction Studies Using XFEM Technique," *Journal of Solid Mechanics*, vol. 6, no. 4, pp. 410-421, 2014. [Google Scholar] [Publisher Link]
- [32] A. Tafreshi, "Computation of the Jk-Integrals for Bimaterial Interface Cracks using Boundary Element Crack Shape Sensitivities," *Theoretical and Applied Fracture Mechanics*, vol. 82, pp. 77-87, 2016. [CrossRef] [Google Scholar] [Publisher Link]
- [33] M.T. Ebrahimi et al., "Discrete Crack Dynamics: A Planar Model of Crack Propagation and Crack-Inclusion Interactions in Brittle Materials," *International Journal of Solids and Structures*, vol. 152-153, pp. 12-27, 2018. [CrossRef] [Google Scholar] [Publisher Link]
- [34] Tiantang Yu, and Tinh Quoc Bui, "Numerical Simulation of 2-D Weak and Strong Discontinuities by a Novel Approach based on XFEM with Local Mesh Refinement," *Composite Structures*, vol. 196, pp. 112-133, 2018. [CrossRef] [Google Scholar] [Publisher Link]
- [35] Al Emran Ismail et al., "Calculating of Stress Intensity Factors of Soldered Joints with Multiple Cracks," *Indonesian Journal of Electrical Engineering and Computer Science*, vol. 14, no. 1, pp. 284-289, 2019. [CrossRef] [Google Scholar] [Publisher Link]
- [36] Eric B. Chin, and N. Sukumar, "Modeling Curved Interfaces without Element-Partitioning in the Extended Finite Element Method," *International Journal for Numerical Methods in Engineering*, vol. 120, no. 5, pp. 607-649, 2019. [CrossRef] [Google Scholar] [Publisher Link]
- [37] Junlei Ding, Tiantang Yu, and Tinh Quoc Bui, "Modeling Strong_Weak Discontinuities by Local Mesh Refinement Variable-Node XFEM with Object-Oriented Implementation," *Theoretical and Applied Fracture Mechanics*, vol. 106, pp. 1-42, 2020. [CrossRef] [Google Scholar] [Publisher Link]
- [38] Achchhe Lal, and Shailesh P. Palekar, "Stochastic Fracture Analysis of Laminated Composite Plate with Arbitrary Cracks using X-FEM," *International Journal of Mechanics and Materials in Design*, vol. 13, pp. 195-228, 2017. [CrossRef] [Google Scholar] [Publisher Link]
- [39] Achchhe Lal et al., "Stochastic Extended Finite Element Implementation for Fracture Analysis of Laminated Composite Plate with a Central Crack," *Aerospace Science and Technology*, vol. 60, pp. 131-151, 2017. [CrossRef] [Google Scholar] [Publisher Link]
- [40] Khubilal Khatri, and Achchhe Lal, "Stochastic XFEM Fracture and Crack Propagation Behavior of an Isotropic Plate with Hole Emanating Radial Cracks Subjected to Various in-Plane Loadings," *Mechanics of Advanced Materials and Structures*, vol. 25, no. 9, pp. 732-755, 2018. [CrossRef] [Google Scholar] [Publisher Link]
- [41] Khubilal Khatri, and Achchhe Lal, "Stochastic XFEM based Fracture Behavior and Crack Growth Analysis of a Plate with a Hole Emanating Cracks under Biaxial Loading," *Theoretical and Applied Fracture Mechanics*, vol. 96, pp. 1-22, 2018. [CrossRef] [Google Scholar] [Publisher Link]
- [42] K.H. Lee, "Stress and Displacement Fields for Propagating the Crack Along the Interface of Dissimilar Orthotropic Materials Under Dynamic Mode I and II Load," *Journal of Applied Mechanics*, vol. 67, no. 1, pp. 223-228, 2000. [CrossRef] [Google Scholar] [Publisher Link]
- [43] Soheil Mohammadi, Extended Finite Element Method: For Fracture Analysis of Structures, Willey, pp. 1-280, 2008. [Google Scholar] [Publisher Link]
- [44] Alireza Asadpoure, Soheil Mohammadi, and Abolhasan Vafai, "Crack Analysis in Orthotropic Media using the Extended Finite Element Method," *Thin Walled Structures*, vol. 44, no. 9, pp. 1031-1038, 2006. [CrossRef] [Google Scholar] [Publisher Link]
- [45] Wen Wang et al., "Numerical Simulation of Interfacial and Subinterfacial Crack Propagation by using Extended Peridynamics," Computers and Structures, vol. 279, 2023. [CrossRef] [Google Scholar] [Publisher Link]
- [46] R. Nikhil et al., "Application of an Instability-Based Fracture Model for Prediction of Crack Initiation in Modified 9Cr–1Mo Steel," Fatigue & Fracture of Engineering Materials & Structures, vol. 48, no. 2, pp. 857-870, 2025. [CrossRef] [Google Scholar] [Publisher Link]
- [47] Ping Li et al., "A Novel Strength-Energy Criterion for Bimaterial Interface Crack Propagation," *International Journal of Solids and Structures*, vol. 298, 2024. [CrossRef] [Google Scholar] [Publisher Link]
- [48] María A. Herrera-Garrido, and Vladislav Mantič, "Stress Singularities in the Generalised Comninou Frictional Contact Model for Interface Cracks in Anisotropic Bimater," *Journal of the Mechanics and Physics of Solids*, vol. 203, 2025. [CrossRef] [Google Scholar] [Publisher Link]
- [49] Shailesh P. Palekar et al., "Probabilistic Fracture Analysis of Double Edge Cracked Orthotropic Laminated Plates using the Stochastic Extended Finite Element Method," *Forces in Mechanics*, vol. 14, pp. 1-17, 2024. [CrossRef] [Google Scholar] [Publisher Link]

Appendix 1: Isotropic Bimaterial Interfaces

Sukumar et al. [12] used methods from Rice [4], Mohammadi S. [46], and other researchers, but they did not consider the effects of contact and crack spreading. They created an approximate solution for cracks in materials that have the same properties throughout. Deng [8] made the basic approximate solution for cracks that happen because of friction, focusing on stationary and moving cracks along the boundary between two different materials in uniform solids, especially looking at the material on top of the boundary (k = 1).

$$\begin{split} u_{x} &= \frac{e^{-\varepsilon(\pi-\theta)} \mathrm{Re}(\bar{K}r)^{i\varepsilon}}{2\mu(1+4\varepsilon^{2}) \cosh(\pi\varepsilon)} \sqrt{\frac{r}{2\pi}} \bigg[-e^{2\varepsilon(\pi-\theta)} \left(\cos\frac{\theta}{2} + 2\varepsilon\sin\frac{\theta}{2}\right) \\ &+ \kappa \left(\cos\frac{\theta}{2} - 2\varepsilon\sin\frac{\theta}{2}\right) + (1+4\varepsilon^{2}) \sin\frac{\theta}{2} \cos\theta \bigg] \\ &+ \frac{e^{-\varepsilon(\pi-\theta)} \mathrm{Im}(\bar{K}r)^{i\varepsilon}}{2\mu(1+4\varepsilon^{2}) \cosh(\pi\varepsilon)} \sqrt{\frac{r}{2\pi}} \bigg[e^{2\varepsilon(\pi-\theta)} \left(\sin\frac{\theta}{2} - 2\varepsilon\cos\frac{\theta}{2}\right) \\ &+ \kappa \left(\sin\frac{\theta}{2} + 2\varepsilon\cos\frac{\theta}{2}\right) + (1+4\varepsilon^{2}) \cos\frac{\theta}{2} \sin\theta \bigg] \\ u_{y} &= \frac{e^{-\varepsilon(\pi-\theta)} \mathrm{Re}(\bar{K}r)^{i\varepsilon}}{2\mu(1+4\varepsilon^{2}) \cosh(\pi\varepsilon)} \sqrt{\frac{r}{2\pi}} \bigg[e^{2\varepsilon(\pi-\theta)} \left(\sin\frac{\theta}{2} - 2\varepsilon\cos\frac{\theta}{2}\right) \\ &+ \kappa \left(\sin\frac{\theta}{2} + 2\varepsilon\cos\frac{\theta}{2}\right) - (1+4\varepsilon^{2}) \cos\frac{\theta}{2} \sin\theta \bigg] \\ &+ \frac{e^{-\varepsilon(\pi-\theta)} \mathrm{Im}(\bar{K}r)^{i\varepsilon}}{2\mu(1+4\varepsilon^{2}) \cosh(\pi\varepsilon)} \sqrt{\frac{r}{2\pi}} \bigg[e^{2\varepsilon(\pi-\theta)} \left(\cos\frac{\theta}{2} + 2\varepsilon\sin\frac{\theta}{2}\right) \\ &- \kappa \left(\cos\frac{\theta}{2} - 2\varepsilon\sin\frac{\theta}{2}\right) + (1+4\varepsilon^{2}) \sin\frac{\theta}{2} \sin\theta \bigg] \end{split} \tag{A2}$$

For the substance over the interface (k = 1), where

$$\kappa = \begin{cases} \frac{3 - \nu}{1 + \nu} & \text{plane stress} \\ 3 - 4\nu & \text{plane strain} \end{cases}$$
 (A3)

And the SIF *K* is,

$$\bar{K} = K_I + iK_{II} \tag{A4}$$

They are characterized similarly to the classical SIF.

$$\left[\sigma_{yy} + i\sigma_{xy}\right]_{\substack{r \to 0 \\ \theta = 0}} = \frac{\bar{K}r^{i\varepsilon}}{\sqrt{2\pi r}}$$
(A5)

K and the rate of energy release can be connected by,

$$G = \frac{1}{E^{12}} \frac{|\bar{K}|^2}{cosh(\pi \varepsilon)} = \frac{1}{E^{12}} \frac{K_I^2 + K_{II}^2}{cosh(\pi \varepsilon)}$$
(A6)

Where each material's effective Young's modulus $E_{k}^{'}$ (k = 1, 2) defines the equivalent bimaterial elastic modulus, or E^{12}

$$E' = \begin{cases} \frac{E}{E} & \text{Plane Stress} \\ \frac{E}{1 - \nu^2} & \text{Plane Strain} \end{cases}$$

$$\frac{2}{E^{12}} = \frac{1}{E_1'} + \frac{1}{E_2'}$$
(A8)

The oscillation index, or ε , is described as

$$\varepsilon = \frac{1}{2\pi} \ln\left(\frac{1-\beta}{1+\beta}\right) \tag{A9}$$

Whereby Dundurs [1969] defines the second Dunder parameter-
$$\beta$$
,
$$\beta = \frac{\mu_1(k_2-1) - \mu_2(k_1-1)}{\mu_1(k_2+1) + \mu_2(k_1+1)} \tag{A10}$$

By substituting $-\varepsilon\pi$ for $\varepsilon\pi$, investigation - A1 and A2 may be applied to a point in the lower half plane.

The angle of phase ψ , measured r away from the crack tip, is another significant measure used in defining interfacial fracture.

$$\psi = tan^{-1} \left[\frac{lm(\bar{K}r^{i\varepsilon})}{Re(\bar{K}r^{i\varepsilon})} \right] \tag{A11}$$
 According to Sukumar et al. [12], the angle of phase ψ represents the shear proportion of normal traction forces at a

distance r away from the crack tip.